Published online 23 September 2014 *Nucleic Acids Research, 2014, Vol. 42, No. 20* ***e159***
doi: 10.1093/nar/gku850

A real-time fluorescence polarization activity assay to screen for inhibitors of bacterial ribonuclease P

Xin Liu[1], Yu Chen[1] and Carol A. Fierke[1,2,*]

[1]Department of Chemistry, University of Michigan, Ann Arbor, MI 48109, USA and [2]Department of Biological Chemistry, University of Michigan Medical School, Ann Arbor, MI 48109, USA

Received August 12, 2014; Revised September 4, 2014; Accepted September 5, 2014

ABSTRACT

Ribonuclease P (RNase P) is an essential endonuclease that catalyzes the 5′ end maturation of precursor tRNA (pre-tRNA). Bacterial RNase P is an attractive potential antibacterial target because it is essential for cell survival and has a distinct subunit composition compared to the eukaryal counterparts. To accelerate both structure-function studies and discovery of inhibitors of RNase P, we developed the first real-time RNase P activity assay using fluorescence polarization/anisotropy (FP/FA) with a 5′ end fluorescein-labeled pre-tRNA^{Asp} substrate. This FP/FA assay also detects binding of small molecules to pre-tRNA. Neomycin B and kanamycin B bind to pre-tRNA^{Asp} with a K_d value that is comparable to their IC_{50} value for inhibition of RNase P, suggesting that binding of these antibiotics to the pre-tRNA substrate contributes to the inhibitory activity. This assay was optimized for high-throughput screening (HTS) to identify specific inhibitors of RNase P from a 2880 compound library. A natural product derivative, iriginol hexaacetate, was identified as a new inhibitor of *Bacillus subtilis* RNase P. The FP/FA methodology and inhibitors reported here will further our understanding of RNase P molecular recognition and facilitate discovery of antibacterial compounds that target RNase P.

INTRODUCTION

In the maturation pathway for transfer RNA (tRNA), the cleavage of the 5′ end leader from precursor tRNAs (pre-tRNAs) is catalyzed by ribonuclease P (RNase P) (1,2). RNase P also catalyzes cleavage of various non-tRNA substrates (3) including pre-4.5S RNA (4), pre-tmRNA (5), mRNAs (6–8) and riboswitches (9,10). In most organisms, RNase P is a ribonucleoprotein consisting of a single catalytic RNA subunit (P RNA) and variable numbers of protein subunits depending on the organism (1 in Bacteria, ≥4 in Archaea and ≥9 in Eukarya nuclei) (11). Recently, solely protein-based RNase P enzymes have been identified in human mitochondria (12), the plant *Arabidopsis thaliana* (13,14), and some algae and protists (15,16). Because of its essential role in RNA processing and the differential subunit composition from its eukaryal counterparts, bacterial RNase P is a potential antibacterial drug target (17,18).

Several reported inhibitors of *Escherichia coli* RNase P are well-known ribosomal antibiotics, including puromycin ($IC_{50} \sim 3$ mM) (19), aminoglycosides (e.g. neomycin B, $IC_{50} = 60$ μM) (20), and neomycin B derivatized with arginine, lysine or guanidinium moieties (IC_{50} values ranging from 0.1 to 6 μM) (21,22). The usefulness of these aminoglycoside derivatives *in vivo* may be limited by their high positive charge that may lead to promiscuous binding to nucleic acids. Aminoglycosides are also weak non-competitive inhibitors of eukaryal RNase P ($K_i = 143$ μM for neomycin B to *Dictyostelium discoideum* RNase P) (23). A number of synthetic compounds, including bis-benzimidazoles ($IC_{50} =$ 5–21 μM) (24), porphines and porphyrins ($K_i = 1$–4 μM) (25), inhibit *E. coli* RNase P activity mainly through binding to pre-tRNA. Spiramycin, a macrolide antibiotic, was reported to activate the steady-state turnover catalyzed by *E. coli* RNase P (26). Recently, a small molecule has been suggested to bind to the protein component of *Staphylococcus aureus* RNase P (*Rnp*A) to alter mRNA turnover and pathogenesis (27). Virtual screening of the ZINC database (28) has proposed additional inhibitors of RNase P that function by disrupting interactions between the pre-tRNA substrate and the P protein subunit (18). Inhibitors of RNase P have also been designed using an antisense approach, targeting P RNA for *E. coli* and *Bacillus subtilis* RNase P ($IC_{50} = 2$ nM–1 μM) (29–32). However, the antisense nucleic acids have to be conjugated with invasive peptides to enter bacterial cells and target RNase P *in vivo* (32). To further evaluate bacterial RNase P as a viable drug target, more potent and specific inhibitors of bacterial RNase P need to be discovered and characterized.

Conventional methods for measuring RNase P activity and inhibition mainly analyze cleavage of ^{32}P-labeled pre-tRNAs using denaturing polyacrylamide gel electrophoresis and phosphorimager quantification (20). These radio-

*To whom correspondence should be addressed. Tel: +1 734 936 2678; Fax: +1 734 647 4865; Email: fierke@umich.edu

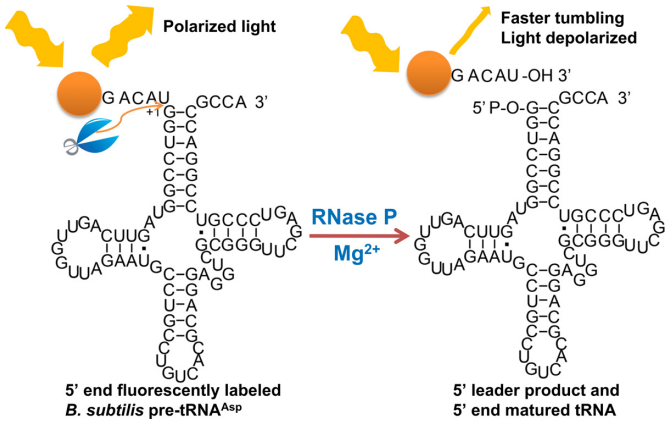

Figure 1. A fluorescence polarization/anisotropy assay for measuring RNase P-catalyzed pre-tRNA cleavage. A fluorescein dye (orange dot) is attached to the 5′ end of a *Bacillus subtilis* pre-tRNA^{Asp} with a 5-nt leader (Fl-pre-tRNA^{Asp}). When excited with polarized light, the Fl-pre-tRNA^{Asp} tumbles slower than the lifetime of the fluorophore so that the emitted light remains polarized (high anisotropy). Upon cleavage of the 5′ end leader catalyzed by RNase P, the Fl-5nt-leader product rotates faster leading to enhanced depolarization of the emitted light (lower anisotropy).

chemical assays are discontinuous, labor-intensive and relatively low-throughput. Fluorescence techniques provide an attractive non-radioactive approach to measure RNase P activity. Previously, substrate binding and transient kinetics of *B. subtilis* RNase P have been measured using a fluorescein-labeled pre-tRNA^{Asp} (33–35). The sensitivity and signal dynamic range of this assay are sufficient for single-turnover (STO) experiments but not for measuring steady-state kinetics (34). Furthermore, bacterial RNase P activity has been measured by fluorescence polarization (FP) using hybridization of fluorescently labeled oligonucleotides to the cleaved 5′ leader product in a discontinuous format (36). To accelerate the identification and analysis of inhibitors of RNase P, a non-radioactive and real-time assay is desirable.

Here we describe the development of a real-time fluorescence polarization/anisotropy (FP/FA) assay for analyzing RNase P activity using a 5′ fluorescein-labeled pre-tRNA^{Asp} substrate (Fl-pre-tRNA^{Asp} (33), Figure 1). This FP/FA assay measures RNase P activity in a continuous format, and is suitable for high-throughput screening (HTS) of RNase P inhibitors, as well as detecting ligands that interact with pre-tRNA. To validate this FP/FA assay, we measured inhibition of *B. subtilis* RNase P by two previously reported *E. coli* RNase P inhibitors, neomycin B (NeoB) and kanamycin B (KanB) (20), demonstrating IC_{50} values in the micromolar range. The FP/FA assay also indicates that both of these inhibitors bind to pre-tRNA with micromolar affinity, suggesting that inhibition of RNase P is at least partly due to binding to the substrate. Finally, we used this assay for a pilot high-throughput screen for RNase P inhibitors and identified a new *in vitro* inhibitor of *B. subtilis* RNase P, irriginol hexaacetate, with IC_{50} and K_i values in the nanomolar range. These data demonstrate that the FP/FA assay facilitates both analysis of pre-tRNA processing catalyzed by RNase P and screening for inhibitors of RNase P.

MATERIALS AND METHODS

Chemicals and reagents

Nucleotide triphosphates (NTP), spermidine and other chemicals were obtained from Sigma at the highest purity unless otherwise indicated. Sodium dodecyl sulfate (SDS) and tRNA^{mix} from baker's yeast were purchased from Fisher Scientific. Inorganic pyrophosphatase was purchased from Roche Applied Science. Guanosine 5′-monothiophosphate (GMPS) was synthesized from 2′, 3′ isopropylidene-guanosine and thiophosphoryl chloride as described (37). Recombinant His_6-T7 RNA polymerase was expressed in *E. coli* and purified by Ni-NTA chromatography as described previously (38).

Preparation of RNA and P protein

The P protein and P RNA subunits of *B. subtilis* RNase P were prepared as previously described (39,40). Fl-pre-tRNA^{Asp} containing a 5-nucleotide leader sequence (Figure 1) was prepared using procedures adapted from previous reports (33,35). Pre-tRNA^{Asp} with a 5′ monothiophosphate terminus was transcribed in the presence of 4 mM adenosine triphosphate (ATP), cytidine triphosphate (CTP), uridine triphosphate (UTP), 4–5 mM GMPS and 0.8–1 mM guanosine triphosphate (GTP), 0.1 μg/μl T7 RNA polymerase, 0.8–1 μg/μl linearized DNA template, 1 mM spermidine, 5 mM dithiothreitol (DTT), 2 μg/ml pyrophosphatase, 50 mM Tris–HCl (pH 8.0) and 20–28 mM $MgCl_2$, incubated at 37°C either overnight (20 mM $MgCl_2$) or for 4–6 h with addition of 20 μM NTPs every 30 min (28 mM $MgCl_2$). The transcribed 5′-GMPS-pre-tRNA^{Asp} was buffer exchanged and concentrated using ≥3 iterations of centrifugal filtration (Amicon Ultra, 10 000 MWCO, Millipore Corporation) into a degassed labeling buffer [10 mM Tris–HCl, pH 7.2, 1 mM ethylenediaminetetraacetic acid (EDTA)] at 4°C and then incubated with 20- to 40-fold excess of 5-IAF (5-Iodoacetamido-fluorescein, Life Technologies) at 37°C overnight to obtain Fl-pre-tRNA^{Asp}. Radiolabeled substrate was prepared by incubating pre-tRNA^{Asp} with calf intestinal alkaline phosphatase New England Biolabs (NEB) followed by 5′ end-labeling using T4 polynucleotide kinase (NEB) and [γ-^{32}P] ATP and purified as described (41). All RNAs were purified by electrophoresis on a 6% (P RNA) or 10% (pre-tRNA^{Asp}) polyacrylamide/bis (39:1) denaturing gel containing 7 M urea. Excised RNA bands were soaked into buffer containing 10 mM Tris-HCl pH 8, 1 mM EDTA, 0.1% SDS, and 500 mM NaCl at 4°C overnight. Eluted RNA was filtered, concentrated and exchanged using centrifugal filtration into buffer containing 10 mM Tris-HCl pH 8, 1 mM EDTA and 500 mM NaCl and then ethanol precipitated for storage at −80°C. Before use, P RNA and pre-tRNA^{Asp} were denatured by heating for 3 min at 95°C in autoclaved Milli-Q water and then refolded by incubating at 37°C for 10–15 min followed by addition of reaction buffer and incubation for at least 30 min. Then P protein was added to the P RNA for a 30 min incubation at 37°C to form the holoenzyme.

Single- and multiple-turnover experiments

The following buffers were prepared immediately before use for enzyme assays: Buffer A (50 mM Tris/MES pH 5.5, 10 mM $MgCl_2$, 200 mM KCl, 20 mM DTT); Buffer B (50 mM Tris–HCl pH 7.2, 10 mM $MgCl_2$, 100 mM KCl, 20 mM DTT); Buffer C (buffer B at pH 8); HTS buffer [similar to buffer B except for 5 mM $MgCl_2$, 12 mg/ml yeast $tRNA^{Mix}$, 10 mM spermidine and 0.01% (v/v) nonidet P-40 (NP-40)]. The pH of stock buffer solution was measured at 25°C.

For gel assays, time points for the cleavage reaction catalyzed by RNase P were taken by diluting aliquots of the reaction into an equal volume of a quenching solution [10 M urea, 200 mM EDTA (pH 8.0), 0.005% (w/v) bromophenol blue and 0.005% (w/v) xylene cyanol] as described (41). The pre-$tRNA^{Asp}$ and 5′ leader product were separated using a 10% denaturing gel and visualized using a Typhoon phosphorimager. The percentage of cleavage was quantified by ImageQuant 5.2 or ImageJ software.

Real-time FP/FA cleavage assays were performed in a black 96-well microplate (Corning Incorporation, #3915 or #3686) by monitoring the FP/FA signal of fluorescein (λ_{ex} = 485 nm and λ_{em} = 535 nm) using a TECAN plate-reader (Genois, G-factor = 0.95, or Infinite F500, G-factor = 0.94). The reactions were initiated by addition of either the enzyme or substrate. Experiments measuring STO reactions were carried out using excess enzyme concentration ([E] = 360 to 500 nM, [S] = 10 to 25 nM) in buffer A at 37°C. The STO cleavage rate constant (k_{obs}) was calculated by fitting Equation (1) to the percentage cleaved (Y) progress curves calculated from the change in FA signal using Equation (2):

$$Y = Y_\infty(1 - e^{-k_{obs}t}) \quad (1)$$

$$Y = 1 - \frac{r - r_\infty}{r_0 - r_\infty + (g-1)(r_0 - r)} \quad (2)$$

Because of total fluorescence change, Equation (2) was used to adjust the percent cleavage during STO reaction by the enhancement factor, $g = F^0/F^\infty$, where F^0 and F^∞ are the total florescence of RNase P holoenzyme-bound substrate and cleaved product, and r_0 and r_∞ are the anisotropy values of the holoenzyme-bound substrate and cleaved product, respectively (42,43).

The multiple-turnover (MTO) measurements of RNase P activity were performed under excess substrate ([S] = 0.01 to 1 μM, [E] = 0.1 to 1 nM) in buffer B, buffer C or HTS buffer. The substrate-only controls were included on each plate and the FP/FA trace of the substrate-only control was subtracted from reaction traces to adjust for temperature variation. The linear initial rates in millianisotropy per second (mA/s) from the time courses were converted to reaction velocity (nM/s) using Equation (3) (44) where: $\Delta r_t/\Delta t$ is the initial rate and Δr_c is the FA signal change upon complete conversion of substrate to product.

$$v_0 = \frac{\left(\frac{\Delta r_t}{\Delta t}\right)}{\Delta r_c}[S] \quad (3)$$

Steady-state kinetic parameters, k_{cat}, K_M and k_{cat}/K_M were calculated from a fit of the Michaelis–Menten equation (45) to the dependence of the initial reaction velocity on the concentration of Fl-pre-$tRNA^{Asp}$. All data analyses were performed using Prism 5.03 (GraphPad Software).

IC_{50} and mode of inhibition experiments

The dose-response curves for inhibition of MTO cleavage catalyzed by RNase P were measured as described in figure and table legends using 96-well microplate FA assays. The enzyme and substrate concentrations were kept constant with varying inhibitor concentrations (Figure 6B). Assays measuring inhibition by NeoB and KanB were performed in the absence of dimethyl sulfoxide (DMSO) because aminoglycosides are highly soluble in aqueous solution. The iriginol hexaacetate (Ir6Ac, MicroSource Discovery Systems, Inc.) inhibitor was dissolved in DMSO and 1% DMSO was included in the reaction for all inhibitor concentrations. The initial rates in the DMSO blank (MIN inhibition = 100% activity) and in the presence of 20 mM $CaCl_2$ or without enzyme (MAX inhibition = 0% activity) were used as negative and positive controls for inhibition, respectively, to calculate the percent activity using Equation (4), where *Inh* is the initial rate at a given inhibitor concentration:

$$\%\text{Activity} = \frac{Inh - MAX}{MIN - MAX} \times 100 \quad (4)$$

The concentration of an inhibitor that results in 50% loss of the enzyme activity (IC_{50}) was calculated using Equation (5) where n is the Hill coefficient:

$$\%\text{Activity} = \frac{100}{1 + \left(\frac{[I]}{IC_{50}}\right)^n} \quad (5)$$

To determine the mode of inhibition of Ir6Ac, the apparent steady-state kinetic parameters were calculated from a fit of the Michaelis–Menten equation to the dependence of the RNase P cleavage activity on the concentration of Fl-pre-$tRNA^{Asp}$ under various concentrations of the inhibitor. Equation (6) was fit to the dependence of the $k_{cat,app}$ and $(k_{cat}/K_M)_{app}$ parameters on the concentrations of Ir6Ac to determine inhibition constants and cooperativity (Figure 7A and B). A mixed inhibition model (Equation 7) was used to globally fit all of the data using GraphPad Prism 5.03 software to generate one best-fit value of parameters. Other models of inhibition (noncompetitive, competitive and uncompetitive) were globally fit to the data and the goodness of fit was compared based on R^2 values (Supplementary Table S1).

$$k_{app} = \frac{k}{1 + \frac{[I]^n}{K_i^n}}; \quad k = k_{cat,app} \text{ or } \left(\frac{k_{cat}}{K_M}\right)_{app} \quad (6)$$

$$\frac{v_0}{[E]} = \frac{\frac{k_{cat}}{\left(1 + \frac{[I]^{n_{is}}}{K_{is}^{n_{is}}}\right)}[S]}{\frac{\left(1 + \frac{[I]^{n_i}}{K_i^{n_i}}\right)}{\left(1 + \frac{[I]^{n_{is}}}{K_{is}^{n_{is}}}\right)}K_M + [S]} \quad (7)$$

Dissociation constant determined by FA

The dissociation constant of aminoglycosides (neomycin B or kanamycin B) for Fl-pre-tRNA^{Asp} was measured from the dependence of the FA signal on the inhibitor concentration (Figure 4A). The compounds were incubated with 50 nM Fl-pre-tRNA^{Asp} at 37°C for 15 min in the plate-reader before collecting data. Equation (8) was fit to the titration curve to obtain the dissociation constant, K_d, where r_f is the anisotropy of unbound Fl-pre-tRNA^{Asp} and B_{max} is the difference in FA between free and fully bound Fl-pre-tRNA^{Asp}·compound complex.

$$Y = r_f + \frac{B_{max} \times [I]}{K_d + [I]} \quad (8)$$

Calculation of anisotropy in relation to molecular weight

A theoretical dependence of FA on the molecular weight of the fluorescein-labeled pre-tRNA^{Asp} (Figure 8) was calculated according to Stoke's (Equation 9) and Perrin equations (Equation 10) [(43) and references therein], where r_0 is the limiting anisotropy in the absence of depolarization factors, T is the fluorescence lifetime, θ is rotational correlation time, η is viscosity, M is molecular weight, R is gas constant $= 8.31 \times 10^7$ erg/K/mol, $\bar{v}$ is theoretical volume for globular protein and h is the degree of hydration. The data (solid line) in Figure 8 was generated by applying $r_0 =$ 222 mA, $T = 4$ ns, $\eta = 0.0069$ P, $R = 8.31 \times 10^7$erg/K/mol, $T = 310$ K, $\bar{v} = 0.75$ ml/g and $h = 0.2$ (46).

$$\theta = \frac{\eta V}{RT} = \frac{\eta M}{RT}(\bar{v} + h) \quad (9)$$

$$\frac{1}{r} = \frac{1}{r_0} + \frac{\tau}{r_0 \theta} \quad (10)$$

High-throughput screening

To develop the end-point HTS assay, RNase P cleavage reactions were carried out at 30°C in a black 384-well microplate (Corning Corporation, #3676). The enzyme was pre-incubated with 2% DMSO for 30 min, then reaction was initiated by addition of an equal volume of substrate and quenched by the addition of 80 mM $CaCl_2$ at various times (Figure 5A). The FP was measured using a PheraStar plate reader (BMG Labtech) with a FP filter module ($\lambda_{ex} =$ 485 nm and $\lambda_{em} = 520$ nm).

The HTS library (~2880 compounds) was provided by the Center for Chemical Genomics (CCG) at University of Michigan. For the primary compound screen, reactions were carried out using final concentrations of 10 μM compound, 1% DMSO, 0.15 nM RNase P (2 nM P protein) and 20 nM Fl-pre-tRNA^{Asp} at 30°C in HTS buffer [50 mM Tris–HCl pH 7.2, 5 mM $MgCl_2$, 100 mM KCl, 20 mM DTT, 12 mg/ml yeast tRNA^{Mix}, 10 mM spermidine and 0.01% (v/v) NP-40]. The enzyme was added using a Multidrop Combi reagent dispenser with a micro-multidrop cassette (Thermo Fisher) and then each compound (in DMSO) or DMSO alone (negative controls) was pinpointed into the solution by Biomek FX Pintool (Beckman Coulter). For the positive control wells, 80 mM $CaCl_2$ was added immediately. RNase P was incubated with compounds at 30°C for 30 min before reactions were initiated by addition of Fl-pre-tRNA^{Asp} substrate. The plates were incubated for another 35 min at 30°C before addition of $CaCl_2$ to quench the reactions. The microplates were read using the PheraStar plate reader using well H23 of each plate to adjust the gain and beam position.

The robustness of the HTS assay was evaluated by calculating the Z′-factor according to Equation (11), where σ_{c+} and σ_{c-} stand for standard deviation for positive and negative controls respectively and μ_{c+} and μ_{c-} are the average values from positive and negative controls. As seen from the Equation (11), the Z′-factor is a screening window coefficient and is defined as the ratio of the separation band to the signal dynamic range of the assay (47).

$$Z' = 1 - \frac{(3\sigma_{c+} + 3\sigma_{c-})}{|\mu_{c+} - \mu_{c-}|} \quad (11)$$

From the primary screen, compounds with percent inhibition values of greater than or equal to three times standard deviation (3SD) of the negative controls were defined as active. Additionally, samples with fluorescence intensity (perpendicular channel) of greater or less than 3SD of negative controls were considered false positives. Promiscuous compounds, as identified by previous HTS in the MScreen database (appears as hits in ≥21% of screens recorded in CCG), were also excluded from further study. Using these triage rules, 252 compounds were selected for further analysis.

A confirmation screen of the 252 compounds identified compounds that bind to pre-tRNA. Briefly, the compound samples in triplicate were incubated with Fl-pre-tRNA^{Asp} substrate and the FP signal was read before addition of RNase P. Alteration of the FP signal of Fl-pre-tRNA^{Asp} (more than 3SD of negative controls) was used to identify compounds that bind substrate. Compounds that repeatedly showed 30% or more inhibition activity and were not identified as pre-tRNA binders were defined as active inhibitors. Next a dose-response screen of active compounds was carried out by varying the concentration of inhibitor from 1 to 10 μM. Samples that showed a concentration-dependent inhibitory activity (Equation 5) were identified as active. Iriginol hexaacetate (Ir6Ac) was the only active hit from the confirmation screen. Ir6Ac was further tested for inhibition of RNase P-catalyzed cleavage using a radioactive gel-based assay (41). 100 nM unlabeled and <0.4nM ^{32}P-pre-tRNA^{Asp} substrate was mixed with 0.2 nM RNase P and varying concentrations of Ir6Ac (0, 5 and 10 μM), incubated for 35 min at room temperature and quenched by addition of EDTA. Cleavage was analyzed on a 10% denaturing gel. Ir6Ac inhibited RNase P (>3SD of negative control) in this radioactivity assay.

RESULTS

Fluorescence polarization/anisotropy to measure pre-tRNA cleavage

We developed a real-time FP/FA assay for measuring RNase P activity. In general, FP/FA assays measure the degree of polarization of a fluorophore, reflecting the rotational time of the fluorophore, which varies with molecular

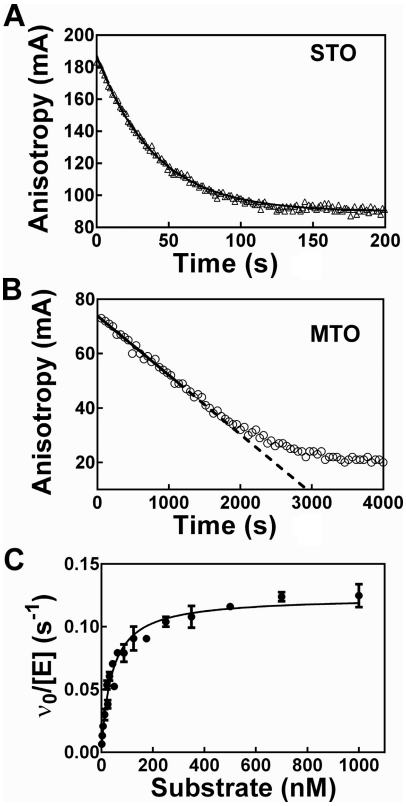

Figure 2. Measurement of pre-tRNA cleavage catalyzed by RNase P using fluorescence anisotropy (FA). (**A**) The time-dependent change in FA was measured under single-turnover (STO) conditions in buffer A (50 mM Tris/MES pH 5.5, 10 mM $MgCl_2$, 200 mM KCl, 20 mM DTT) with 25 nM Fl-pre-tRNA^{Asp} and 500 nM *Bacillus subtilis* RNase P holoenzyme at 37°C. The solid line is a single exponential fit to the data with k_{obs} = 0.0250 ± 0.0002 s^{-1}; when Equation (2) was used to adjust for the change in total florescence and Equation (1) was fit to the data, the k_{obs} = 0.032 ± 0.001 s^{-1}. (**B**) The time-dependent change in FA was measured under multiple-turnover (MTO) conditions in buffer C (50 mM Tris–HCl pH 8, 10 mM $MgCl_2$, 100 mM KCl, 20 mM DTT) with 20 nM Fl-pre-tRNA^{Asp}, 0.4 nM *B. subtilis* RNase P and 4 nM P protein at 37°C. Total fluorescence does not change for multiple turnover reactions. The steady-state cleavage velocity is measured from the linear initial rate (solid line). (**C**) Steady-state kinetic parameters were determined from the dependence of the MTO initial rate on substrate concentration. Reaction conditions are the same as in B except for varying RNase P (0.3–1 nM) and Fl-pre-tRNA^{Asp} (2 nM–1 μM) concentrations. Results are from three independent experiments and the error bars are the standard deviations. The Michaelis–Menten equation was fit to the data yielding: k_{cat} = 0.124 ± 0.003 s^{-1}, K_M = 40 ± 3 nM, k_{cat}/K_M = 3100 ± 200 $mM^{-1}s^{-1}$.

Table 1. Comparison of RNase P cleavage activity measured by different assays

Assay methods	STO[a] rate constant k_{obs} (s^{-1})	MTO[b] velocity v_0 (nM·s^{-1})
FA real-time assay	0.032 ± 0.001	2.2 ± 0.1
Fluorescence gel assay	0.033 ± 0.006	
^{32}P gel assay		1.9 ± 0.1

[a]Measured in buffer A (50 mM Tris/MES pH 5.5, 10 mM $MgCl_2$, 200 mM KCl, 20 mM DTT) with 25 nM Fl-pre-tRNA^{Asp}, 500 nM holoenzyme at 37°C.
[b]Measured in HTS buffer [50 mM Tris–HCl pH 7.2, 10 mM $MgCl_2$, 100 mM KCl, 20 mM DTT, 12 mg/ml yeast tRNA^{Mix}, 10 mM spermidine and 0.01% (v/v) NP-40] by 100 nM Fl-pre-tRNA^{Asp} or 100 nM unlabeled pre-tRNA^{Asp} mixed with <0.4 nM ^{32}P-pre-tRNA^{Asp} substrate, 0.15 nM holoenzyme and 1.5 nM of P protein at 25°C.

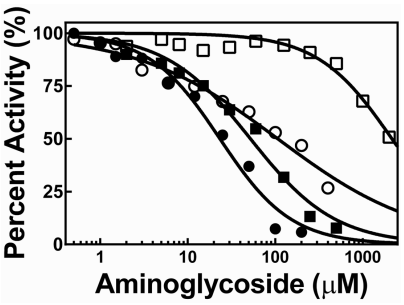

Figure 3. Neomycin B and kanamycin B inhibit *Bacillus subtilis* RNase P. Dose-response of RNase P inhibition was measured in buffer B (50 mM Tris–HCl pH 7.2, 10 mM $MgCl_2$, 100 mM KCl, 20 mM DTT) with 50 nM Fl-pre-tRNA^{Asp} and 0.4 nM RNase P with 4 nM P protein at 37°C. The concentrations for NeoB (•) and KanB (■) that inhibit activity by 50% (IC_{50}, Equation 5) are 23 ± 3 μM (n = 1.1 ± 0.1) and 52 ± 6 μM (n = 0.9 ± 0.1), respectively. In the presence of 12 mg/ml yeast tRNA^{Mix}, the IC_{50} values for NeoB (○) and KanB (□) are 110 ± 20 μM (n = 0.53 ± 0.05) and 2.2 ± 0.3 mM (n = 1.0 ± 0.2), respectively.

mass, solvent viscosity and excited state lifetime [(43) and reference therein]. FP/FA measures the ratio of parallel and perpendicular light so the assay is ratiometric, sensitive, independent of the substrate concentration, highly accurate (error <5% even with just a 2-fold dynamic range) (43) and easy to adapt to a high-throughput mode (48). We used a 5′ end fluorescein labeled pre-tRNA^{Asp} (Fl-pre-tRNA^{Asp} (33), Figure 1) to measure cleavage catalyzed by *B. subtilis* RNase P using FP/FA. The experimentally measured FP/FA signal of Fl-pre-tRNA^{Asp} substrate (high anisotropy) and the Fl-5-nt leader product (low anisotropy) differ by 2 to 3-fold, providing a wide dynamic range for the cleavage assay (Figure 2). Cation concentration and buffer composition also affect the FP/FA signal of Fl-pre-tRNA^{Asp} as shown in Supplementary Figure S1, likely by altering the mobility of the fluorophore through stabilizing the pre-tRNA structure (49). When *B. subtilis* RNase P is mixed with Fl-pre-tRNA^{Asp} a time-dependent decrease in the FP/FA signal is observed under both single- ([E]/[S]>10, Figure 2A) and MTO ([S]/[E] > 10, Figure 2B) conditions. Similar FA reaction curves have been observed for RNase P-catalyzed cleavage of 5′ fluorescein labeled pre-tRNA^{Asp} with 2, 7 and 10-nucleotide leaders (data not shown). The STO cleavage rate constant and the MTO reaction velocity determined using the FP/FA assay are nearly identical to the values determined from the gel assay (Table 1). Furthermore, the steady-state kinetic parameters measured using the FA assay (k_{cat} = 0.124 ± 0.003 s^{-1}, K_M = 40 ± 3 nM, k_{cat}/K_M = 3100 ± 200 $mM^{-1}s^{-1}$, Figure 2C) are in the same range as previously reported values for cleavage of pre-tRNA^{Asp} (41). Therefore, the real-time FP/FA signal accurately measures the cleavage activity of RNase P.

Table 2. Inhibition of RNase P by neomycin B and kanamycin B is decreased by addition of yeast $tRNA^{Mix}$ and spermidine

	NeoB		KanB	
Assay condition	IC_{50}	K_d	IC_{50}	K_d
Buffer B[a]	23 ± 3 μM	90 ± 5 μM	52 ± 6 μM	220 ± 20 μM
+12 mg/ml Yeast $tRNA^{b}$	110 ± 20 μM	100 ± 20 μM	2.2 ± 0.3 mM	540 ± 60 μM
+10 mM Spermidine[c]	>1 mM[d]	>1 mM[d]	>1 mM[d]	>1 mM[d]

[a]Measured in buffer B (50 mM Tris–HCl pH 7.2, 10 mM $MgCl_2$, 100 mM KCl, 20 mM DTT) and with 50 nM Fl-pre-$tRNA^{Asp}$, 0.4 nM holoenzyme and 4 nM P protein at 37°C as described in Figure 3.
[b]Same as [a] except with 12 mg/ml yeast $tRNA^{Mix}$ in the buffer.
[c]Same as [a] except with 12 mg/ml yeast $tRNA^{Mix}$ and 10 mM spermidine in the buffer.
[d]<20% inhibition or binding was observed at this concentration measured.

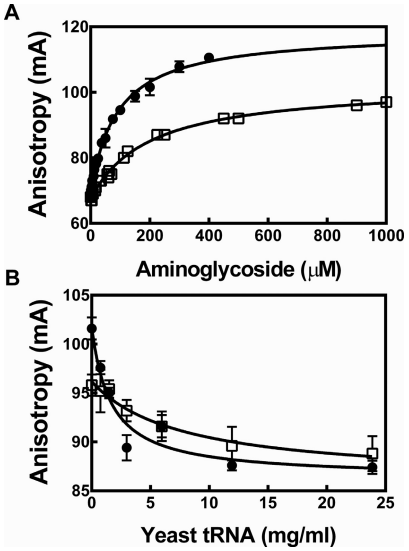

Figure 4. Neomycin B and kanamycin B bind to Fl-pre-$tRNA^{Asp}$. (**A**) The FA of Fl-pre-$tRNA^{Asp}$ increases upon titration with NeoB (•) and KanB (□), measured in buffer B as described in legend of Figure 3 at 37°C with 50 nM FI-pre-$tRNA^{Asp}$. The K_d values for NeoB and KanB are determined from a fit of Equation (8) to these data as 90 ± 5 μM and 220 ± 20 μM, respectively. (**B**) Yeast $tRNA^{Mix}$ competes with Fl-pre-$tRNA^{Asp}$ for binding neomycin B and kanamycin B using either 200 μM NeoB (•) or 1 mM KanB (□) and varying concentrations of yeast $tRNA^{Mix}$ in buffer B. Error bars show the standard deviations from five replicates.

Neomycin B and kanamycin B inhibit *B. subtilis* RNase P and bind to pre-tRNA substrate

To test the utility of this assay for identifying and evaluating inhibitors of RNase P, we measured inhibition of *B. subtilis* RNase P by two previously reported aminoglycoside inhibitors, neomycin B (NeoB) and kanamycin B (KanB) (20) (Figure 3). Both NeoB and KanB inhibit *B. subtilis* RNase P cleavage activity with IC_{50} values of 23 and 52 μM, respectively (Table 2). These IC_{50} values are comparable to those measured for inhibition of *E. coli* RNase P (20).

Interestingly, an enhancement in the FA signal is observed when NeoB or KanB is titrated into Fl-pre-$tRNA^{Asp}$ alone (Figure 4) while the total fluorescence intensity was constant. This result suggests that these inhibitors bind to Fl-pre-$tRNA^{Asp}$. Apparent dissociation constants (K_d, Table 2) were obtained from fitting a hyperbolic curve (Equation 8) to the FA titration curve (Figure 4A). The K_d of NeoB (90 μM) agrees well with the published value for the affinity of NeoB for a native yeast $tRNA^{Phe}$ (K_d = 90 μM) (49). Furthermore, the affinity of NeoB (K_d = 90 μM) and KanB (K_d = 220 μM) are similar to the IC_{50} values measured for inhibition of RNase P (IC_{50} = 23 and 52 μM, respectively), suggesting that the binding of these compounds to the Fl-pre-tRNA substrate contributes to RNase P inhibition. This conclusion is bolstered by the observed decrease in the FP/FA signal when yeast $tRNA^{Mix}$ is titrated into the Fl-pre-$tRNA^{Asp}$·aminoglycoside complex (Figure 4B). Furthermore, yeast $tRNA^{Mix}$ decreases the affinity of NeoB and KanB for Fl-pre-$tRNA^{Asp}$ by up to 3-fold and increases the IC_{50} for inhibition of RNase P by NeoB and KanB by 5-fold and >40-fold, respectively (Figure 3 and Table 2). These data further suggest that aminoglycoside binding to pre-tRNA plays a role in RNase P inhibition.

Inhibition of *B. subtilis* RNase P by NeoB is decreased by addition of 10 mM spermidine (Table 2) or 100 mM Mg^{2+} (data not shown), consistent with previous studies of inhibition of *E. coli* RNase P by aminoglycosides (20,21). Furthermore, addition of spermidine increases the FA signal for Fl-pre-$tRNA^{Asp}$ to a level comparable to that of saturating NeoB (~110 mA, Supplementary Figure S1). This is likely due to the previously observed effect of polyamine in stabilizing tRNA (49).

Optimization of assay conditions for high-throughput screen

A matrix of conditions was tested to optimize the end-point FP assay in 384-well microplates for HTS. First we analyzed commonly used HTS reagents. *B. subtilis* RNase P activity is inhibited 20% by 2% DMSO and unaffected by non-ionic detergent NP-40 (0.01–0.1% v/v) (Supplementary Figures S1 and S2). Therefore, the final DMSO concentration was limited to 1%. Second, we optimized the robustness of HTS assays, indicated by the Z′-factor (47). FP measures the same phenomenon as FA (43). However, we used the FP signal in the high-throughput screens because it provides a larger dynamic range for signal, leading to an improvement in the Z′-factor (Equation 11). Quenching the reaction by addition of 80 mM $CaCl_2$ rather than EDTA further enhanced the FP signal dynamic range because the FP signal of Fl-pre-$tRNA^{Asp}$ is dependent on the tRNA structure. Addition of EDTA decreases the FP value for Fl-pre-$tRNA^{Asp}$ by ~30 mP thus decreasing signal dynamic range. Therefore $CaCl_2$ was used as a quench because $CaCl_2$ slows

cleavage by ~10^4-fold (50) (Figure 5A) and only slightly increases FP signal of the Fl-pre-tRNA^{Asp} substrate but not the product (data not shown). Finally, the concentration of Fl-pre-tRNA^{Asp} substrate in the HTS was set to the value of K_M (20 nM) to allow detection of both competitive and uncompetitive inhibitors and a low concentration of RNase P holoenzyme (0.15 nM) was used so that the reaction has a linear range of ~30 min (Figure 5A). Furthermore, yeast tRNA^{Mix} and spermidine were included in the HTS assay to reduce nonspecific binding to nucleic acids and to enhance identification of inhibitors that bind to RNase P rather than pre-tRNA^{Asp} substrate.

Using the established optimum conditions for the endpoint FP assay, a high-throughput screen of a library of ~2880 compounds was carried out in 384-well microplates (nine plates). The ~2880 compound library (MS200 + NCC set), containing bioactive small molecules and natural products of known chemical formula, is a pilot set for evaluating assay performance. The 9 plates in this primary screen have an average Z'-factor of 0.76 (Figure 5B), demonstrating that the assay is robust for high-throughput screens (47). Furthermore, orthogonal radioactivity cleavage assays confirmed inhibitors identified from the FP screens. The assay conditions decreased the hit rate from 2–5% (in the absence of spermidine and yeast tRNA^{Mix}) to 0.1% by minimizing non-specific binding to pre-tRNA^{Asp} and thereby increasing the identification of inhibitors that specifically bind to RNase P.

Iriginol hexaacetate (Ir6Ac) inhibits RNase P

From the 2880 compound library, Ir6Ac is the only compound that was confirmed as an inhibitor for *B. subtilis* RNase P through multiple screens (Figure 6). The IC_{50} of Ir6Ac for inhibition of *B. subtilis* RNase P in HTS buffer is 820 ± 10 nM (Figure 6B). In addition, titration of Ir6Ac into Fl-pre-tRNA^{Asp} does not affect the FA signal, indicating that this compound does not bind to Fl-pre-tRNA^{Asp} (data not shown). These data suggest that Ir6Ac is a reversible inhibitor of RNase P with higher specificity than previously reported inhibitors, such as neomycin B.

To evaluate the mechanism of inhibition of *B. subtilis* RNase P by Ir6Ac, we measured the MTO activity of RNase P as a function of both Ir6Ac and Fl-pre-tRNA^{Asp} concentration (Figure 7C). The values of the steady-state kinetic parameters of RNase P-catalyzed cleavage in the HTS conditions are: $k_{cat} = 0.157 \pm 0.002$ s^{-1}, $K_M = 15 \pm 1$ nM, $k_{cat}/K_M = 10200 \pm 600$ mM^{-1}s^{-1} (Figure 7C). The addition of Ir6Ac decreases the values of k_{cat}, K_M and k_{cat}/K_M, indicating a mixed inhibition model (inhibitor binds to both enzyme, E, and enzyme-substrate complex, ES, with different affinity). Furthermore, in comparison to other models (competitive, noncompetitive or uncompetitive) the mixed inhibition model has the smallest error and highest R^2 value (0.9775) in a weighted global fitting of RNase P activity under varying concentrations of Ir6Ac and substrate (Equation 7; $n_i = n_{is} = 1$; Figure 7C and D). Ir6Ac leads to substantial decreases in the apparent value of k_{cat}/K_M with possible positive cooperativity, as indicated by a slightly more robust fit of the data with an n_i of 1.4 ± 0.1 compared to $n = 1$ (Equation 6; Figure 7A). Nonetheless, the inhibition constants determined by either a cooperative or non-cooperative ($n_i = n_{is} = 1$) model are comparable (Supplementary Table S1). Therefore, these data reveal that Ir6Ac inhibits *B. subtilis* RNase P by mixed inhibition with inhibition constants of $K_i = 130 \pm 10$ nM and $K_{is} = 480 \pm 30$ nM with $n_i = n_{is} = 1$ (Figure 7C and D).

DISCUSSION

To facilitate mechanistic studies and discovery of inhibitors of bacterial RNase P, we have developed a high-throughput FP/FA assay that can measure both cleavage activity of RNase P in real-time and binding of small ligands to tRNA. The FP/FA assay is safer and more cost-effective than the radioactivity-based assay and measures activity with high precision since it is ratiometric. A previously reported stopped FP/FA assay for RNase P hybridizes the cleaved 5′ leader product to a fluorescently labeled oligonucleotide (36). The real-time FP/FA assay reported here does not require separation of substrate and product or quenching of the reaction. The 96- or 384-well plate assay format facilitates measurement of RNase P activity under multiple conditions and identification of inhibitors. The HTS FP assay is robust and cost-effective for large scale high-throughput screens.

FP/FA for measuring compound binding to pre-tRNA

The correlation between FA and molecular weight is estimated from the Perrin equation (Equation 10), indicating that a large molecule (higher molecular weight) will have a longer rotational correlation time (Equation 9) and thus higher anisotropy (Equation 10). The rotational correlation time is calculated using the Stoke's equation (Equation 9) by assuming a rigid attachment model for the fluorophore to a spherical macromolecule (43). Calculations using this model recapitulate the experimental values for the Fl-5-nt-leader product and the fully bound Fl-pre-tRNA^{Asp}·RNase P complex. However, the experimental FA reading for Fl-pre-tRNA^{Asp} is ~70 mA, which is significantly smaller than the predicted theoretical value of ~140 mA (Figure 8). Previous studies also reported low FA signal for 3′ end-labeled fluorescein tRNA^{fmet} (51) and 5′ end-labeled peptidyl-tRNA (52). Unexpectedly, a significant change in anisotropy (>30 mA) occurred upon binding of NeoB (M.W. = 614.6 g/mol, ΔFA ~ 50 mA) or KanB (483.3 g/mol, ΔFA ~ 35 mA) to Fl-pre-tRNA^{Asp}. (Figure 4A). This is in contrast to predictions by the Perrin equation indicating that binding a small molecular weight compound (<0.1 kDa) to Fl-pre-tRNA^{Asp} (~26 kDa) should generate a negligible change (ΔFA ~ 1 mA) in FA signal. Interestingly, the FA signal of the NeoB or KanB bound complexes approach the theoretical value calculated for Fl-pre-tRNA^{Asp} (Figure 8).

Two scenarios could explain these anomalous results. The low anisotropy values measured for Fl-pre-tRNA^{Asp} could be due to the fluorescein in Fl-pre-tRNA^{Asp} rotating more freely and rapidly than pre-tRNA^{Asp}. Alternatively, pre-tRNA^{Asp} could be more dynamic than a macromolecule of the same molecular weight, rapidly sampling different conformations and rotating more rapidly in solution. The increase in the FA signal observed upon binding NeoB and

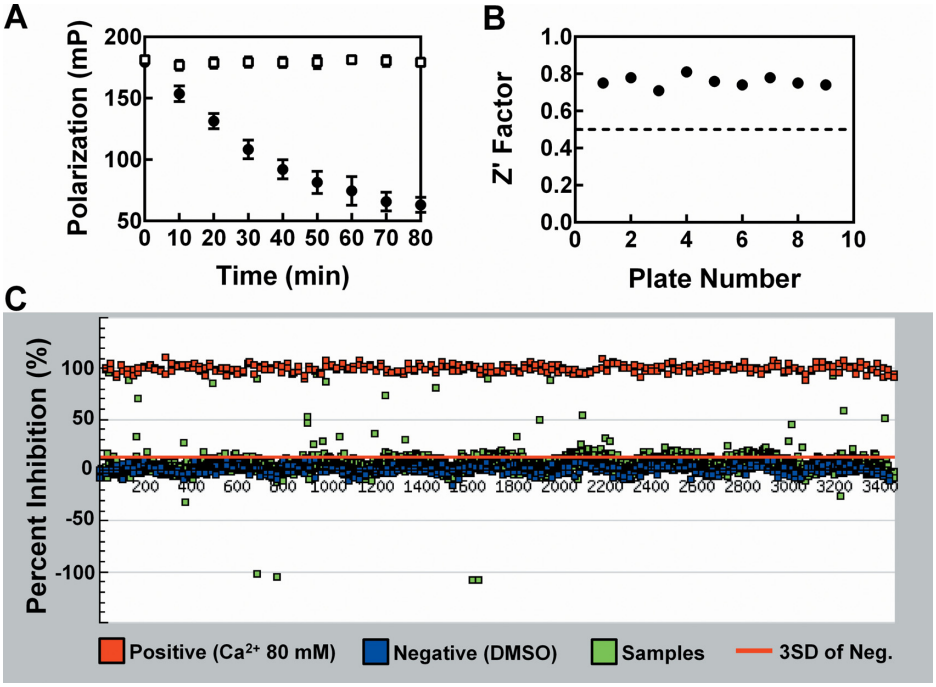

Figure 5. High-throughput FP assay is robust for screening inhibitors of *Bacillus subtilis* RNase P. (**A**) Reaction progress curves measured by quenching the reaction with 80 mM $CaCl_2$ at specified time points in HTS buffer [50 mM Tris–HCl pH 7.2, 5 mM $MgCl_2$, 100 mM KCl, 20 mM DTT, 12 mg/ml yeast $tRNA^{Mix}$, 10 mM spermidine and 0.01% (v/v) NP-40] with 1% DMSO, 20 nM FL-pre-$tRNA^{Asp}$ and 0.15 nM RNase P with 1.5 nM P protein at 30°C. The reactions contained either no inhibitor (1% DMSO blank, •) as a negative control or 80 mM $CaCl_2$ (□) as a positive control for inhibition. Error bars are derived from 18–32 replicates in one 384-well plate. (**B**) The Z′- factor values for the FP HTS assay determined from each of the nine 384-well microplates in primary screen. (**C**) A scatter plot showing the percent inhibition by plate in the primary screen of the 2880 compound library. Positive controls including 80 mM $CaCl_2$ in the assay are shown by red squares. Negative controls (1% DMSO) are blue. Compound samples are green. The red solid line indicates percent inhibition at three times the standard deviation of negative controls (3SD). The samples showing negative inhibition contain compounds interfering with fluorescence signal.

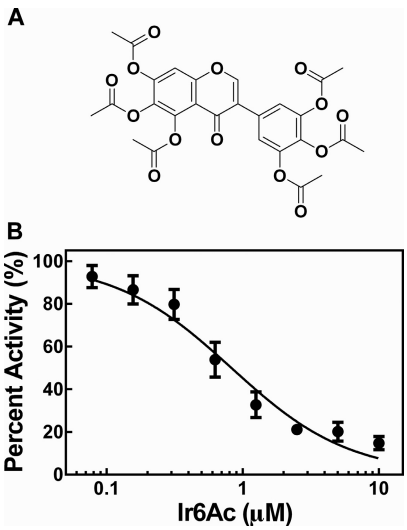

Figure 6. Iriginol hexaacetate inhibits *Bacillus subtilis* RNase P catalyzed cleavage. (**A**) Chemical structure of iriginol hexaacetate (Ir6Ac). (**B**) Dose-response curve of inhibition by Ir6Ac of MTO cleavage activity catalyzed by RNase P measured in HTS buffer with 50 nM Fl-pre-$tRNA^{Asp}$ and 0.1 nM *B. subtilis* RNase P with 2 nM P protein. Ir6Ac was pre-incubated with RNase P for 40 min at 37°C prior to initiation of reaction. IC_{50} is 820 ± 10 nM with a Hill coefficient of 1.0 ± 0.1.

KanB is due to a decrease in the mobility of the fluorescein moiety via a direct interaction or through stabilization of the pre-$tRNA^{Asp}$ structure, which decreases mobility. This latter proposal is consistent with previous observations that these compounds interact with and stabilize $tRNA^{Phe}$ (49,53). The melting temperature (T_m) of native $tRNA^{Phe}$ is increased by complexation with NeoB (49). Furthermore, a 2.6 Å resolution co-crystal structure illustrates that NeoB binds in the deep groove below the D-loop of the yeast $tRNA^{Phe}$, displacing a bound Mg^{2+} (53). This binding site is remote from the 5′ end of tRNA and is unlikely to directly affect the mobility of the fluorescein moiety. Therefore, the low anisotropy signal of free Fl-pre-$tRNA^{Asp}$ likely reflects the dynamic nature of the tRNA. This allows measurement of the binding of ligands, such as aminoglycosides, that stabilize tRNA structure using changes in FA.

Modes of inhibition of RNase P

Mechanisms for inhibition of bacterial RNase P function can be multifold. For example, inhibitors could disrupt the P RNA·P protein association, chelate structurally and functionally important metal ions, alter P RNA conformation, and/or disrupt substrate recognition by binding to either pre-tRNA or RNase P (18). Positively charged compounds could bind to RNA with high affinity but may also be non-specific. To develop specific inhibitors targeting RNase P, it is important to identify compounds that bind to the en-

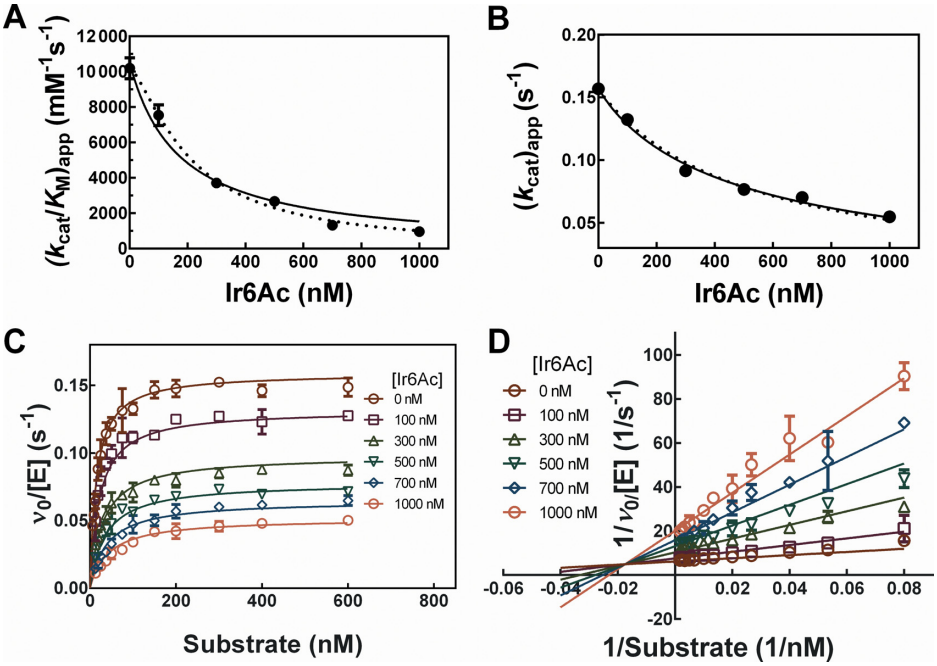

Figure 7. Mechanism of inhibition of *Bacillus subtilis* RNase P by Ir6Ac. The assays were carried out at a fixed RNase P concentration of 0.4 nM (2 nM P protein) with varying concentrations of Ir6Ac and Fl-pre-tRNA^{Asp} in HTS buffer at 37°C. Ir6Ac was pre-incubated with RNase P for 40 min. (**A** and **B**) Fit of Equation (6) to the apparent k_{cat} (A) and k_{cat}/K_M (B) values as a function of concentration of Ir6Ac. The solid line is a fit with $n = 1$ ($R^2 = 0.9731$ for k_{cat}/K_M and 0.9899 for k_{cat}) and the dotted line is a fit where n is a variable: for k_{cat}/K_M, $n = 1.4 \pm 0.1$ ($R^2 = 0.9969$) and for k_{cat}, $n = 0.9 \pm 0.1$ ($R^2 = 0.9919$). (**C**) Best global fit for inhibition of RNase P in the presence of varying concentrations of substrate (6–600 nM). Equation (7) for a non-cooperative mixed inhibition is fit to the data ($R^2 = 0.9775$) with $K_i = 130 \pm 10$ nM and $K_{is} = 480 \pm 30$ nM ($n_i = n_{is} = 1$); (**D**) Lineweaver–Burk plot for the dependence of RNase P activity on Ir6Ac and substrate concentrations. A non-cooperative mixed inhibition model is fit to the data ($R^2 = 0.9670$). Symbols represent means ± SD determined from two to three independent experiments at each concentration.

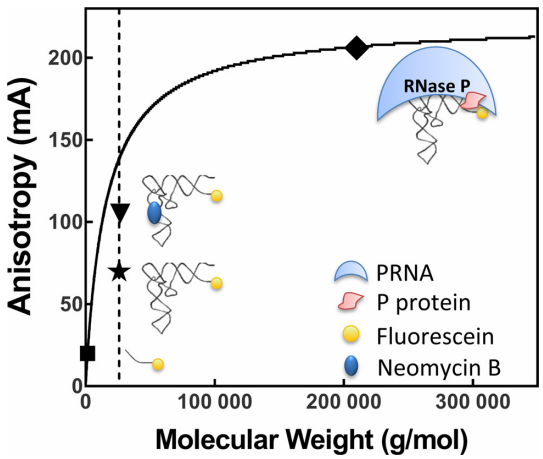

Figure 8. Comparison of the theoretical calculation and experimental results for the FA value of fluorescein labeled pre-tRNA^{Asp}. The dashed line indicates the molecular weight (26,085 g/mol) of pre-tRNA^{Asp} with a 5-nt leader calculated from the sequence in Figure 1. The solid line is the theoretical FA value calculated using Equation (10). The solid symbols indicate the experimental FA values measured in Buffer B (50 mM Tris–HCl pH 7.2, 10 mM $MgCl_2$, 100 mM KCl, 20 mM DTT) except values for Fl-pre-tRNA^{Asp} bound to RNase P were measured in 10 mM $CaCl_2$ and 200 mM KCl at pH 6: Fl-5-nt-leader (■), Fl-pre-tRNA^{Asp} (★), Fl-pre-tRNA^{Asp}•NeoB (▼) and Fl-pre-tRNA^{Asp}•RNase P (♦).

zyme rather than the pre-tRNA substrate. We have demonstrated that the FP/FA assay can detect small ligand binding to pre-tRNA if the interactions alter the solution structure (Figure 4). This assay is more sensitive for measuring small ligands binding to tRNA than previous methods relying on changes in the intrinsic fluorescence of modified bases on native tRNA (49) or of the compounds (24,54,55), and other spectroscopic methods such as UV-VIS and circular dichroism (24,54–56). The FP/FA assay reported here using end-labeled pre-tRNA provides a general and convenient way of measuring binding and stabilization of *in vitro* transcribed tRNA by non-fluorescent molecules. Additionally, this assay identifies ligands that bind to any site that alters the conformational mobility of tRNA. Compounds that stabilize tRNA structure might be of particular interest for drug development (57). For example, tRNA stabilizing agents will be a valuable tool for studying the structure, function and biology of the vast number of pathogenic mutations in human mitochondrial tRNAs (58).

For inhibition of RNase P by aminoglycosides and derivatives previous biochemical and computational docking studies have suggested three possible binding sites on P RNA (21,22,59): (i) the P1-P4 helix junction and J19/4 region to compete with the P protein and/or pre-tRNA; (ii) the P15 loop to compete with Mg^{2+}; and (iii) the P15 region to compete with pre-tRNA. Additionally, both our data and previous structural and biochemical data demonstrate that NeoB and KanB bind to tRNA (49,53), suggesting another possible mechanism of inhibition of RNase P. In fact, the affinity of NeoB and KanB to Fl-pre-tRNA^{Asp} is only 4-fold weaker than the IC_{50} for inhibition of RNase P (Ta-

ble 2). In addition, yeast $tRNA^{Mix}$ significantly decreases inhibition of *B. subtilis* RNase P by NeoB and KanB (≥5-fold; Table 2). Based on these results, we suggest that binding of aminoglycosides to pre-tRNA inhibits RNase P activity, contributing to the observed inhibition of RNase P by these compounds.

Novel RNase P inhibitor

Unlike NeoB and KanB, the newly identified RNase P inhibitor, Ir6Ac, is a potent (IC_{50} = 820 nM) inhibitor of RNase P. The inhibition mechanism of Ir6Ac is mixed indicating that the inhibitor binds to both RNase P (K_i = 130 nM) and the RNase P·pre-$tRNA^{Asp}$ complex (K_{is} = 480 nM). Furthermore, based on FA measurements, this inhibitor does not bind to either pre-$tRNA^{Asp}$ or $tRNA^{Asp}$, suggesting that Ir6Ac is more specific for inhibition of RNase P compared to previously reported compounds such as aminoglycosides which bind to pre-tRNA substrate (Table 2). Ir6Ac is a semisynthetic derivative of irigenol, a member of the isoflavone natural products family produced by higher plants such as *Leguminosae*. Isoflavones, including genistein and daidzein, are suggested to function as phytoestrogens and antioxidants (60). Isoflavones have also been suggested to confer anti-cancer effects (61,62). Recent studies have shown that isoflavone compounds stabilize G-quadruplex but destabilize duplex structure in human telomeric DNA (63), indicating that this class of molecule interacts with nucleic acids. Ir6Ac is unlikely to function *in vivo* because the acetyl groups may be readily hydrolyzed but this scaffold can serve as a lead compound for the development of useful antibacterial compounds targeting RNase P.

Conclusion

RNase P plays an essential role in tRNA biogenesis and is considered a novel antibacterial target (17). However, previous RNase P assays mainly relied on radiochemical methods which limit the capacity for high-throughput screens to discover novel RNase P inhibitors. The FP/FA assay developed in this study is the first non-radioactive method capable of measuring steady-state cleavage activity of bacterial RNase P in real-time as well as detecting small ligand binding to pre-tRNA. The pilot screen identified a new inhibitor, Ir6Ac, for RNase P, demonstrating the utility of the FP/FA-based HTS assay to identify novel RNase P inhibitors.

This FP/FA assay could also be adopted to measure RNase P activity from other organisms, including the protein-only enzymes from human mitochondria and plants, and other tRNA processing enzymes. Important factors in the assay development include design of the substrates, assay conditions and orthogonal assays to confirm that the FP/FA change accurately reflects the enzymatic activity. Furthermore, the FP/FA binding assay using end-labeled pre-tRNA provides a direct method to study binding and stabilizing of pre-tRNA by small molecules, which could facilitate discovery of compounds targeting pathologies related to tRNA.

SUPPLEMENTARY DATA

Supplementary Data are available at NAR Online.

ACKNOWLEDGMENTS

The authors thank Drs Elaina Zverina, Lyra Chang, John Hsieh and Daina Zeng for helpful discussion with the development of the HTS assay and Professors Jason Gestwicki and Anna Mapp for sharing plate-reader instruments. We thank Martha Larsen, Steven Swaney and Paul Kirchhoff at the Center for Chemical Genomics (CCG) at University of Michigan for their help with the compound library screen and data mining. We thank Nancy Wu, Dr Benjamin Jennings and Michael Howard for comments on the manuscript.

FUNDING

National Institute of Health [R01 GM55387 to C.A.F]; Pilot Screen Grant from the Center for Chemical Genomics at the University of Michigan [to C.A.F.]; Rackham Graduate Student Research Grant [to X.L.]. Funding for open access charge: National Institute of Health.
Conflict of interest statement. None declared.

REFERENCES

1. Kazantsev,A.V. and Pace,N.R. (2006) Bacterial RNase P: a new view of an ancient enzyme. *Nat. Rev. Microbiol.*, **4**, 729–740.
2. Walker,S.C. and Engelke,D.R. (2006) Ribonuclease P: the evolution of an ancient RNA enzyme. *Crit. Rev. Biochem. Mol. Biol.*, **41**, 77–102.
3. Hernandez-Cid,A., Aguirre-Sampieri,S., Diaz-Vilchis,A. and Torres-Larios,A. (2012) Ribonucleases P/MRP and the expanding ribonucleoprotein world. *IUBMB Life*, **64**, 521–528.
4. Peck-Miller,K.A. and Altman,S. (1991) Kinetics of the processing of the precursor to 4.5 S RNA, a naturally occurring substrate for RNase P from Escherichia coli. *J. Mol. Biol.*, **221**, 1–5.
5. Komine,Y., Kitabatake,M., Yokogawa,T., Nishikawa,K. and Inokuchi,H. (1994) A tRNA-like structure is present in 10Sa RNA, a small stable RNA from Escherichia coli. *Proc. Natl. Acad. Sci. U.S.A.*, **91**, 9223–9227.
6. Alifano,P., Rivellini,F., Piscitelli,C., Arraiano,C.M., Bruni,C.B. and Carlomagno,M.S. (1994) Ribonuclease E provides substrates for ribonuclease P-dependent processing of a polycistronic mRNA. *Genes Dev.*, **8**, 3021–3031.
7. Li,Y. and Altman,S. (2003) A specific endoribonuclease, RNase P, affects gene expression of polycistronic operon mRNAs. *Proc. Natl. Acad. Sci. U.S.A.*, **100**, 13213–13218.
8. Marvin,M.C., Clauder-Munster,S., Walker,S.C., Sarkeshik,A., Yates,J.R. 3rd, Steinmetz,L.M. and Engelke,D.R. (2011) Accumulation of noncoding RNA due to an RNase P defect in Saccharomyces cerevisiae. *RNA*, **17**, 1441–1450.
9. Altman,S., Wesolowski,D., Guerrier-Takada,C. and Li,Y. (2005) RNase P cleaves transient structures in some riboswitches. *Proc. Natl. Acad. Sci. U.S.A.*, **102**, 11284–11289.
10. Seif,E. and Altman,S. (2008) RNase P cleaves the adenine riboswitch and stabilizes pbuE mRNA in Bacillus subtilis. *RNA*, **14**, 1237–1243.
11. Lai,L.B., Vioque,A., Kirsebom,L.A. and Gopalan,V. (2010) Unexpected diversity of RNase P, an ancient tRNA processing enzyme: Challenges and prospects. *FEBS Lett.*, **584**, 287–296.
12. Holzmann,J., Frank,P., Löffler,E., Bennett,K., Gerner,C. and Rossmanith,W. (2008) RNase P without RNA: identification and functional reconstitution of the human mitochondrial tRNA processing enzyme. *Cell*, **135**, 462–474.
13. Gobert,A., Gutmann,B., Taschner,A., Gossringer,M., Holzmann,J., Hartmann,R.K., Rossmanith,W. and Giege,P. (2010) A single Arabidopsis organellar protein has RNase P activity. *Nat. Struct. Mol. Biol.*, **17**, 740–744.

14. Gutmann,B., Gobert,A. and Giege,P. (2012) PRORP proteins support RNase P activity in both organelles and the nucleus in Arabidopsis. *Genes Dev.*, **26**, 1022–1027.
15. Lai,L.B., Bernal-Bayard,P., Mohannath,G., Lai,S.M., Gopalan,V. and Vioque,A. (2011) A functional RNase P protein subunit of bacterial origin in some eukaryotes. *Mol. Genet. Genomics*, **286**, 359–369.
16. Taschner,A., Weber,C., Buzet,A., Hartmann,R.K., Hartig,A. and Rossmanith,W. (2012) Nuclear RNase P of Trypanosoma brucei: a single protein in place of the multicomponent RNA-protein complex. *Cell Rep.*, **2**, 19–25.
17. Eder,P.S., Hatfield,C., Vioque,A. and Gopalan,V. (2003) Bacterial RNase P as a potential target for novel anti-infectives. *Curr. Opin. Investig. Drugs*, **4**, 937–943.
18. Willkomm,D., Pfeffer,P., Reuter,K., Klebe,G. and Hartmann,R. (2010) In: Liu,F and Altman,S (eds). *Ribonuclease P*. Springer, New York, **10**, pp. 235–256.
19. Vioque,A. (1989) Protein synthesis inhibitors and catalytic RNA Effect of puromycin on tRNA precursor processing by the RNA component of Escherichia coli RNase P. *FEBS Lett.*, **246**, 137–139.
20. Mikkelsen,N.E., Brannvall,M., Virtanen,A. and Kirsebom,L.A. (1999) Inhibition of RNase P RNA cleavage by aminoglycosides. *Proc. Natl. Acad. Sci. U.S.A.*, **96**, 6155–6160.
21. Eubank,T.D., Biswas,R., Jovanovic,M., Litovchick,A., Lapidot,A. and Gopalan,V. (2002) Inhibition of bacterial RNase P by aminoglycoside-arginine conjugates. *FEBS Lett.*, **511**, 107–112.
22. Kawamoto,S.A., Sudhahar,C.G., Hatfield,C.L., Sun,J., Behrman,E.J. and Gopalan,V. (2008) Studies on the mechanism of inhibition of bacterial ribonuclease P by aminoglycoside derivatives. *Nucleic Acids Res.*, **36**, 697–704.
23. Tekos,A., Tsagla,A., Stathopoulos,C. and Drainas,D. (2000) Inhibition of eukaryotic ribonuclease P activity by aminoglycosides: kinetic studies. *FEBS Lett.*, **485**, 71–75.
24. Hori,Y., Bichenkova,E.V., Wilton,A.N., El-Attug,M.N., Sadat-Ebrahimi,S., Tanaka,T., Kikuchi,Y., Araki,M., Sugiura,Y. and Douglas,K.T. (2001) Synthetic inhibitors of the processing of pretransfer RNA by the ribonuclease P ribozyme: enzyme inhibitors which act by binding to substrate. *Biochemistry*, **40**, 603–608.
25. Hori,Y., Rogert,M.C., Tanaka,T., Kikuchi,Y., Bichenkova,E.V., Wilton,A.N., Gbaj,A. and Douglas,K.T. (2005) Porphyrins and porphines bind strongly and specifically to tRNA, precursor tRNA and to M1 RNA and inhibit the ribonuclease P ribozyme reaction. *Biochim. Biophys. Acta*, **1730**, 47–55.
26. Toumpeki,C., Vourekas,A., Kalavrizioti,D., Stamatopoulou,V. and Drainas,D. (2008) Activation of bacterial ribonuclease P by macrolides. *Biochemistry*, **47**, 4112–4118.
27. Olson,P.D., Kuechenmeister,L.J., Anderson,K.L., Daily,S., Beenken,K.E., Roux,C.M., Reniere,M.L., Lewis,T.L., Weiss,W.J., Pulse,M. *et al.* (2011) Small molecule inhibitors of Staphylococcus aureus RnpA alter cellular mRNA turnover, exhibit antimicrobial activity, and attenuate pathogenesis. *PLoS Pathog.*, **7**, e1001287.
28. Irwin,J.J. and Shoichet,B.K. (2005) ZINC–a free database of commercially available compounds for virtual screening. *J. Chem. Inf. Model.*, **45**, 177–182.
29. Willkomm,D., Gruegelsiepe,H., Goudinakis,O., Kretschmer-Kazemi Far,R., Bald,R., Erdmann,V. and Hartmann,R. (2003) Evaluation of bacterial RNase P RNA as a drug target. *Chembiochem*, **4**, 1041–1048.
30. Childs,J.L., Poole,A.W. and Turner,D.H. (2003) Inhibition of Escherichia coli RNase P by oligonucleotide directed misfolding of RNA. *RNA*, **9**, 1437–1445.
31. Gruegelsiepe,H., Willkomm,D.K., Goudinakis,O. and Hartmann,R.K. (2003) Antisense inhibition of Escherichia coli RNase P RNA: mechanistic aspects. *Chembiochem*, **4**, 1049–1056.
32. Gruegelsiepe,H., Brandt,O. and Hartmann,R.K. (2006) Antisense inhibition of RNase P: mechanistic aspects and application to live bacteria. *J. Biol. Chem.*, **281**, 30613–30620.
33. Rueda,D., Hsieh,J., Day-Storms,J.J., Fierke,C.A. and Walter,N.G. (2005) The 5′ leader of precursor tRNAAsp bound to the Bacillus subtilis RNase P holoenzyme has an extended conformation. *Biochemistry*, **44**, 16130–16139.
34. Hsieh,J. and Fierke,C.A. (2009) Conformational change in the Bacillus subtilis RNase P holoenzyme–pre-tRNA complex enhances substrate affinity and limits cleavage rate. *RNA*, **15**, 1565–1577.
35. Hsieh,J., Koutmou,K.S., Rueda,D., Koutmos,M., Walter,N.G. and Fierke,C.A. (2010) A divalent cation stabilizes the active conformation of the B. subtilis RNase P x pre-tRNA complex: a role for an inner-sphere metal ion in RNase P. *J. Mol. Biol.*, **400**, 38–51.
36. Giordano,T. and S.M.A.S.M.A. and Rao,S. J. (2006) Inhibitors of RNase P proteins as antibacterial compounds. US 7001924 B2.
37. Behrman,E.J. (2000) An improved synthesis of guanosine 5‘-monothiophosphate. *J. Chem. Res.-(S)*, 446–447.
38. He,B., Rong,M., Lyakhov,D., Gartenstein,H., Diaz,G., Castagna,R., McAllister,W.T. and Durbin,R.K. (1997) Rapid mutagenesis and purification of phage RNA polymerases. *Protein Expr. Purif.*, **9**, 142–151.
39. Niranjanakumari,S., Stams,T., Crary,S.M., Christianson,D.W. and Fierke,C.A. (1998) Protein component of the ribozyme ribonuclease P alters substrate recognition by directly contacting precursor tRNA. *Proc. Natl. Acad. Sci. U.S.A.*, **95**, 15212–15217.
40. Niranjanakumari,S., Kurz,J.C. and Fierke,C.A. (1998) Expression, purification and characterization of the recombinant ribonuclease P protein component from Bacillus subtilis. *Nucleic Acids Res.*, **26**, 3090–3096.
41. Kurz,J.C., Niranjanakumari,S. and Fierke,C.A. (1998) Protein component of Bacillus subtilis RNase P specifically enhances the affinity for precursor-tRNAAsp. *Biochemistry*, **37**, 2393–2400.
42. Mocz,G., Helms,M.K., Jameson,D.M. and Gibbons,I.R. (1998) Probing the nucleotide binding sites of axonemal dynein with the fluorescent nucleotide analogue 2′(3′)-O-(-N-Methylanthraniloyl)-adenosine 5′-triphosphate. *Biochemistry*, **37**, 9862–9869.
43. Jameson,D.M. and Ross,J.A. (2010) Fluorescence polarization/anisotropy in diagnostics and imaging. *Chem. Rev.*, **110**, 2685–2708.
44. Sem,D.S. and McNeeley,P.A. (1999) Application of fluorescence polarization to the steady-state enzyme kinetic analysis of calpain II. *FEBS Lett.*, **443**, 17–19.
45. Michaelis,L., Menten,M.L., Johnson,K.A. and Goody,R.S. (2011) The original Michaelis constant: translation of the 1913 Michaelis-Menten paper. *Biochemistry*, **50**, 8264–8269.
46. Lakowicz,J.R. (2006) *Principles of Fluorescence Spectroscopy*. 3rd edn, Springer, NY.
47. Zhang,J.H., Chung,T.D.Y. and Oldenburg,K.R. (1999) A simple statistical parameter for use in evaluation and validation of high throughput screening assays. *J. Biomol. Screen*, **4**, 67–73.
48. Lea,W.A. and Simeonov,A. (2011) Fluorescence polarization assays in small molecule screening. *Expert Opin. Drug Discov.*, **6**, 17–32.
49. Kirk,S.R. and Tor,Y. (1999) tRNA(Phe) binds aminoglycoside antibiotics. *Bioorg. Med. Chem.*, **7**, 1979–1991.
50. Smith,D., Burgin,A.B., Haas,E.S. and Pace,N.R. (1992) Influence of metal ions on the ribonuclease P reaction. Distinguishing substrate binding from catalysis. *J. Biol. Chem.*, **267**, 2429–2436.
51. Ferguson,B.Q. and Yang,D.C. (1986) Methionyl-tRNA synthetase induced 3′-terminal and delocalized conformational transition in tRNAfMet: steady-state fluorescence of tRNA with a single fluorophore. *Biochemistry*, **25**, 529–539.
52. Bonin,P.D. and Erickson,L.A. (2002) Development of a fluorescence polarization assay for peptidyl-tRNA hydrolase. *Anal. Biochem.*, **306**, 8–16.
53. Mikkelsen,N.E., Johansson,K., Virtanen,A. and Kirsebom,L.A. (2001) Aminoglycoside binding displaces a divalent metal ion in a tRNA-neomycin B complex. *Nat. Struct. Biol.*, **8**, 510–514.
54. Bichenkova,E.V., Sadat-Ebrahimi,S.E., Wilton,A.N., O'Toole,N., Marks,D.S. and Douglas,K.T. (1998) Strong, specific, reversible binding ligands for transfer RNA: comparison by fluorescence and NMR spectroscopies with distamycin binding for a new structural class of ligand. *Nucleos. Nucleot.*, **17**, 1651–1665.
55. Basu,A., Jaisankar,P. and Suresh Kumar,G. (2013) Binding of the 9-O-N-aryl/arylalkyl amino carbonyl methyl substituted berberine analogs to tRNA(phe.). *PLoS One*, **8**, e58279.
56. Islam,M.M., Pandya,P., Kumar,S. and Kumar,G.S. (2009) RNA targeting through binding of small molecules: studies on t-RNA binding by the cytotoxic protoberberine alkaloid coralyne. *Mol. Biosyst.*, **5**, 244–254.
57. Tor,Y. (2003) Targeting RNA with small molecules. *Chembiochem*, **4**, 998–1007.

58. Suzuki,T., Nagao,A. and Suzuki,T. (2011) Human mitochondrial tRNAs: biogenesis, function, structural aspects, and diseases. *Annu. Rev. Genet.*, **45**, 299–329.
59. Berchanski,A. and Lapidot,A. (2008) Bacterial RNase P RNA is a drug target for aminoglycoside-arginine conjugates. *Bioconjug. Chem.*, **19**, 1896–1906.
60. Dixon,R.A. (2004) Phytoestrogens. *Annu. Rev. Plant Biol.*, **55**, 225–261.
61. Khan,S.A., Chatterton,R.T., Michel,N., Bryk,M., Lee,O., Ivancic,D., Heinz,R., Zalles,C.M., Helenowski,I.B., Jovanovic,B.D. *et al.* (2012) Soy isoflavone supplementation for breast cancer risk reduction: a randomized phase II trial. *Cancer Prev. Res.*, **5**, 309–319.
62. Nechuta,S.J., Caan,B.J., Chen,W.Y., Lu,W., Chen,Z., Kwan,M.L., Flatt,S.W., Zheng,Y., Zheng,W., Pierce,J.P. *et al.* (2012) Soy food intake after diagnosis of breast cancer and survival: an in-depth analysis of combined evidence from cohort studies of US and Chinese women. *Am. J. Clin. Nutr.*, **96**, 123–132.
63. Zhang,J.L., Fu,Y., Zheng,L., Li,W., Li,H., Sun,Q., Xiao,Y. and Geng,F. (2009) Natural isoflavones regulate the quadruplex-duplex competition in human telomeric DNA. *Nucleic Acids Res.*, **37**, 2471–2482.